

Far- and Near-Field Investigations on the Lasing Modes in Two-Dimensional Photonic Crystal Slab Lasers

Dong-Jae Shin, Se-Heon Kim, Jeong-Ki Hwang, Han-Youl Ryu, Hong-Gyu Park, Dae-Sung Song, and Yong-Hee Lee

Abstract—We present experimental investigations on the lasing modes in two-dimensional (2-D) hexagonal cavities defined by photonic crystals on slab waveguide structures. The far-field emission patterns and near-field intensity distributions of the lasing modes are analyzed in polarization-resolved 2-D angular distribution measurements and spectrally resolved near-field scanning optical microscopy. The far- and near-field analyses result in identification of the various lasing modes and their subsequent classification into one- and two-dimensional modes. In the one-dimensional modes oscillating between two parallel boundaries of the cavities, longitudinal and transverse modes are identified and found to have transverse-electric polarization. In the two-dimensional modes oscillating two-dimensionally in the cavities, various modes including whispering-gallery-like modes are observed and found to exhibit various polarization states.

Index Terms—Far-field, near-field, photonic crystal, semiconductor laser, whispering-gallery-like mode.

I. INTRODUCTION

PHOTONIC crystals (PCs) are an optical analogy of semiconductor crystals which have a periodic potential for electrons [1]. In PCs, the periodic potential for photons is realized by introducing periodic structures of dielectric properties on the scale of optical wavelengths. An important characteristic of these structures is the presence of photonic band gaps (PBGs) in which propagating electromagnetic modes are forbidden. The existence of PBGs results in various applications such as lasers, light-emitting diodes, planar waveguides, and channel-drop filters.

In particular, it has been predicted that spontaneous emission properties of light-emitting materials can be controlled by PCs [2]. This implies that more efficient lasers of desired properties such as low threshold and high modulation speed are obtainable by suitably incorporating PC structures into lasers. As initial trials, there have been great efforts to realize lasers with microcavities defined by PCs. So far, successful lasing has been achieved by several groups with two-dimensional (2-D) PC structures [3]–[10]. A Caltech group has demonstrated lasing action in a cavity formed by a single-defect PC structure [3], [4]. Continuous and room-temperature operation of such lasers with larger cavities has been achieved by a KAIST group [5], [6]. In addition, there have been reports on lasing action

with organic [7]–[9] and semiconductor [10] gain materials in 2-D PC structures of the distributed feedback (DFB) type in which no cavity exists.

In the aforementioned PC lasers, light is confined by the PBG in two dimensions and by total internal reflection of the slab waveguide structure in the third dimension. Theoretically, properties of resonant modes such as polarization, frequency, symmetry, and field distribution have been studied by numerical methods [11]–[15]. On the other hand, there have been no experimental investigations directly addressing such properties of lasing modes. This is mainly because the detailed information is hardly accessible by conventional measurements. For DFB-type PC lasers, out-of-plane diffractive coupling of lasing modes has been discussed based for far-field emission measurements [16].

Conventional methods for characterizing radiation sources exploit far-field imaging systems typically using lenses and charge-coupled device (CCD) cameras. Such systems, however, are able to capture only part of the emission into a certain range of directions, so that an overall investigation of the emission pattern is not possible for highly divergent sources. Moreover, since polarization analyses are usually conducted on emission integrated by the lens, directionally dependent polarization structures are averaged out in most cases. In fact, such polarization structures do appear heavily in small radiation sources such as PC lasers. For the characterization of small radiation sources in the near-field regime, a near-field scanning optical microscope (NSOM) is destined for this purpose. Near-field intensity distributions can be directly measured by scanning a subwavelength-sized probe over the surface of the source with super-resolution beyond the diffraction limit. However, the presence of the probe typically within a few nanometers inevitably perturbs the radiation source so that the resultant measurement reflects the effect of the probe. This problem is more serious for active radiation sources such as microcavity lasers than passive ones such as small metal apertures. In order to avoid this problem, it is desirable to carry out both of the far- and near-field investigations which are complementary to each other [17].

In this paper, we describe initial experiments on 2-D PC slab defect lasers in the far- and near-field regime. In the next section, we present experimental setups for far- and near-field measurements. The third section is devoted to discussions of emission patterns, polarization characteristics, and the symmetry of lasing modes in the far-field regime. The next section is devoted to the near-field regime in which we present for the first time spectrally resolved near-field images of resonant modes.

Manuscript received August 27, 2001; revised November 19, 2001. This work was supported by the National Research Laboratory Project of Korea.

The authors are with the Department of Physics, Korea Advanced Institute of Science and Technology, Taejeon, Korea.

Publisher Item Identifier S 0018-9197(02)05689-0.

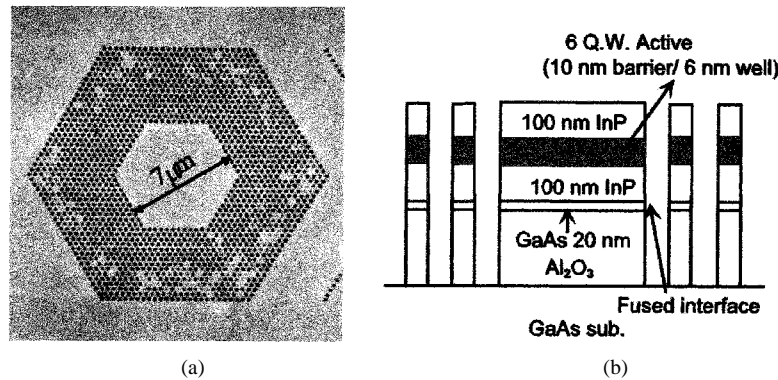


Fig. 1. Structure of a 2-D PC slab defect laser. (a) SEM images of the PC-defined microcavity. (b) Schematic of the slab structure.

II. EXPERIMENTS

The 2-D PC laser is built on a thin InGaAsP slab waveguide structure. The high-index ($n = 3.4$) active layer containing compressively strained multiple quantum wells is sandwiched by air and a low-index ($n = 1.5$) Al_2O_3 layer. In the horizontal plane, a 2-D triangular PC is formed by drilling holes in a triangular lattice. A scanning electron microscope (SEM) image of a typical laser sample and schematic diagram of its slab structure are shown in Fig. 1. The thickness of the slab is 326 nm, which supports a fundamental mode and next higher mode for transverse-electric (TE) polarization [15]. For transverse-magnetic (TM) polarization, only one fundamental mode is allowed. Because of the compressive strain at the quantum wells, coupling to the TM mode is greatly suppressed. In addition, the next higher order TE mode is also suppressed because this mode has a node at the center of the slab. Details of the fabrication are available in [5] and [18]. All the cavities used in the experiments are hexagons in triangular lattices as shown in Fig. 1(a). The triangular lattice of the air columns has been chosen since it presents a relatively large PBG for TE polarization. In order to indicate the cavity size, we designate the cavities as to how many holes they lack in the K direction of the triangular lattice. For example, the cavity in Fig. 1(a) is called a 21-defect cavity.

The experimental setup for far-field measurements is shown in Fig. 2. In order to freely characterize laser emission onto the front side of the laser structure, an external pumping laser beam is illuminated on the back side of the substrate. It should be noted that this back-side pumping is allowed by the transparency of a GaAs substrate for a 980-nm pumping laser beam. Since the cavity sizes are usually less than $10 \mu\text{m}$ and the pumping beam is focused through the substrate containing many layers of different materials, fine alignment of the pumping beam is critical to achieve lasing conditions. Moreover, the lasing modes hop to different modes depending on a slight change of the pumping conditions. Therefore, we have been able to selectively excite different modes by adjusting the pumping alignment and measure the emission patterns of the modes separately.

Because of poor thermal characteristics of the lasers, especially those with small cavities, the pumping laser is modulated by current pulses of typically 10 ns and a 5-MHz repetition rate. For lock-in detection, we superpose another modulation of 740 Hz which is the maximum modulation frequency of the infrared detector used in the measurements. The time constant of

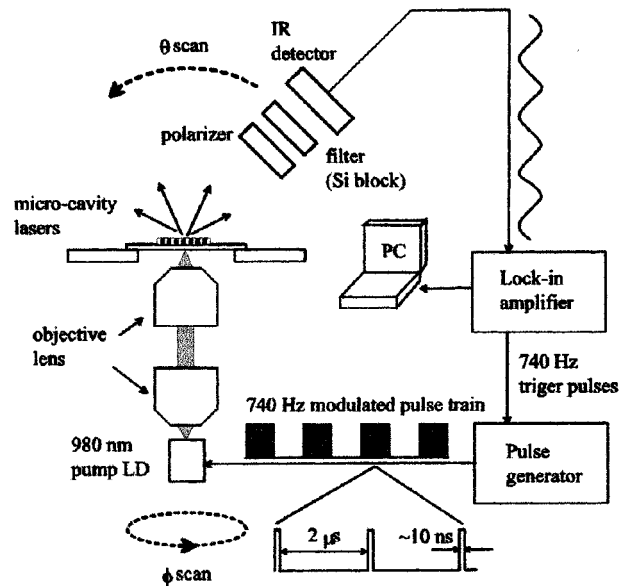


Fig. 2. Experimental setup for far-field measurements on microcavity lasers.

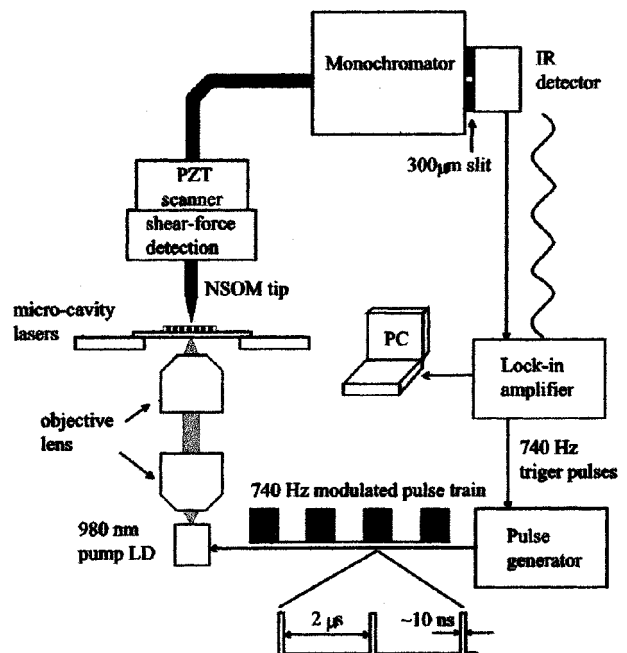


Fig. 3. Experimental setup for near-field measurements on microcavity lasers.

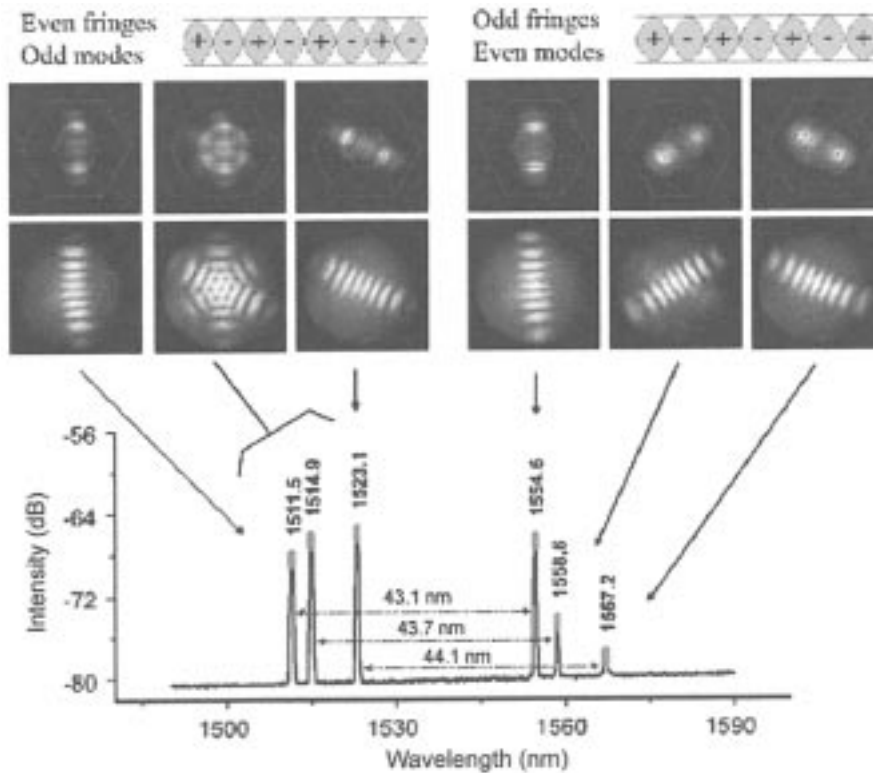


Fig. 4. The CCD near-field patterns (first row), the far-field emission patterns (second row), and the spectrum (bottom graph) of six lasing modes observed with the 2-D PC laser shown in Fig. 1. The dotted lines overlaid in the CCD near-field patterns indicate the physical boundaries defined by the 2-D PC. The second mode from the left is a multimode superimposed by the three left modes shown in the spectrum. The distances between the modes oscillating along the same directions are indicated in the spectrum.

lock-in detection is 300 ms, and the detector waits for 1.5 s at each direction before measurements are made. The dynamic range of the measurements is estimated to be over 1000. The silicon block is placed in front of the detector to filter out the pumping beam. The detector scans from 0° to 90° in the θ direction and from 0° to 360° in the ϕ direction, respectively. We adjust the angular resolution of scanning high enough to resolve the structures of interest observed in the angular distributions. The typical resolution is 2° for the θ direction and 3.6° for the ϕ direction.

In this paper, the data over the curved surface of the spheres (θ, φ) are represented on a 2-D flat surface (x, y) by a simple mapping defined by

$$\theta = \pi \sqrt{x^2 + y^2}$$

$$\varphi = \text{Arg}(x + yi).$$

Please note that the vertical direction [$\theta = 0^\circ$] corresponds to the center of the flat surface (x, y). The range of the polar angles is varied depending on the source structure. This mapping is not linear so that it produces some distortion, especially in a region of high polar angle. In this paper, all 2-D far-field radiation patterns are presented using this mapping.

Fig. 3 shows the experimental setup for near-field measurements. The pumping configuration is the same as that for the far-field measurements. We use uncoated tapered fiber probes fabricated by heating and the subsequent pulling of $1.5\text{-}\mu\text{m}$ single-mode fibers. The sharpness of the probes is approximated to be 100 nm in topography. In order to place and scan the probes in near-field regimes, the distance between

the probe and the sample surface is regulated within about 10 nm by a nonoptical shear-force detection technique using two quartz crystal tuning forks [19]. The light collected by the probe in the near-field regime is guided to the monochromator to be spectrally resolved. Then the intensity is measured by the infrared detector with a $300\text{-}\mu\text{m}$ input slit, which determines the spectral resolution to be 3 nm. The time constant of the lock-in detection is 100 ms and the probe waits for 200 ms at each point before measurements. The dynamic range of the measurements is estimated to be over 100.

III. FAR-FIELD RESULTS

A. One-Dimensional Modes

The 2-D PC lasers sustain various resonant modes and only a few of them lase in most cases. As the cavity size increases, the number of resonant modes increases rapidly. One important issue is what kind of resonant modes lase under what conditions, such as the values of the lattice constant and air-hole radius. In the investigations on various 2-D PC lasers, we identify several lasing modes and classify them into two categories: 1-D modes and 2-D modes.

1) *Longitudinal Mode*: The 1-D lasing modes observed in the 21-defect cavity described in Fig. 1(a) are shown in Fig. 4. Here, the lattice constant is 370 nm, and the hole radius is about $0.33a$, where a is the lattice constant. It should be noted that, while the lattice constant is measured by SEM images with high precision, hole radius is not. This is because the hole shapes are not perfectly circular and not uniform over the lattice as can be

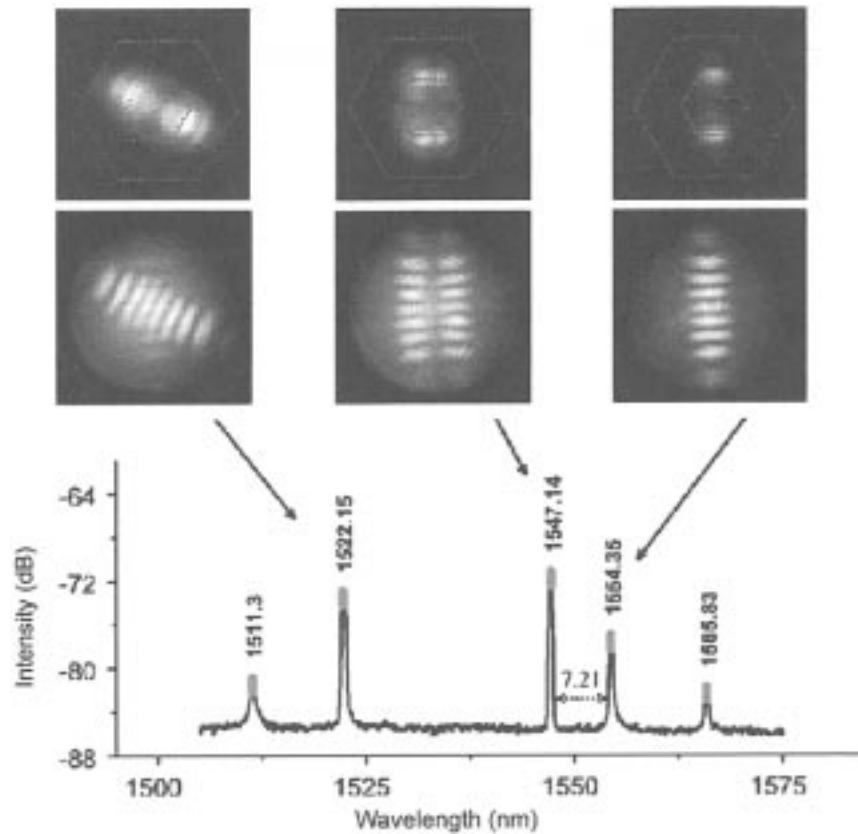


Fig. 5. The CCD near-field patterns (first row), the far-field emission patterns (second row), and the spectrum (bottom graph) of lasing modes observed in the same laser structure shown in Fig. 1. The dotted lines overlaid in the CCD near-field patterns indicate the physical boundaries defined by the 2-D PC. The distance between the two modes oscillating along the same directions are indicated in the spectrum.

confirmed in Fig. 1(a). However, this nonuniformity does not change the results significantly [20]. In fact, we show this figure intentionally to emphasize the robustness of the PC against the imperfections in nanofabrication.

For the laser sample, six lasing modes are observed. By adjusting the pumping conditions, each single mode except the mode at 1514.9 nm is selectively excited and inspected by the far-field measurement setup and an infrared CCD camera. The CCD near-field images show that the laser emission is mainly from two regions at the parallel boundaries of the cavity. The 2-D far-field emission patterns are elongated in the direction normal to the boundaries and contain interference fringes parallel to the boundaries. The two kinds of images consistently indicate that these modes are plane-wave-like modes oscillating between parallel boundaries in the 2-D hexagonal cavity. The three-fold degeneracy inherent in triangular lattices has been lifted in this laser sample by the imperfection of a real device.

The spectrum shows that the six modes form two groups of three modes, each of which corresponds to each of three equivalent M directions of the triangular lattice. The left (right) group has an even (odd) number of fringes. This means that the left (right) group has an even (odd) number of antinodes of standing waves inside the cavity so that the two strong regions are 180° out of phase (in phase), as illustrated in the top of Fig. 4. Therefore, the left (right) group is odd (even) modes which are anti-symmetric (symmetric) under a mirror operation in the longitudinal direction. This observation clearly guarantees that the

modes in the two groups are adjacent longitudinal modes which are separated by a free spectral range in the spectrum. The free spectral ranges for three pairs of 1-D modes for each direction are 43.1, 43.7, and 44.1, respectively, as shown in Fig. 4. Using a group refractive index of 3.0, these values correspond to an effective cavity length of 9.09, 9.01, and 9.02 μm , which are about 129% of the geometric cavity length. The 29% increase implies that the lasing modes decay within a few periods in the PC region.

2) *Transverse Mode*: For the 21-defect cavity in which the lattice constant is 370 nm and the hole radius is about $0.37a$, the transverse mode profiles are shown in Fig. 5. Among the 1-D modes described above, the mode at 1547.14 nm is found to have a node at its center in a transverse direction. The spectral distances and the numbers of fringes indicate that the modes at 1511.3 nm and 1522.15 nm are higher longitudinal modes of the modes at 1554.35 nm and 1565.83 nm, respectively, and the mode at 1547.14 nm is a higher transverse mode of the mode at 1554.35 nm. The higher (lower) transverse mode is an odd (even) mode which is anti-symmetric (symmetric) under a mirror operation in the transverse direction. The spectral separation between the two adjacent transverse modes is found to be 7.21 nm.

3) *1-D Angular Distribution*: As a function of pumping power, cross sections of the 2-D emission patterns of a typical 1-D mode are shown in Fig. 6. The laser has the same structure described in Fig. 1(a). The angular resolution is 0.2° in this

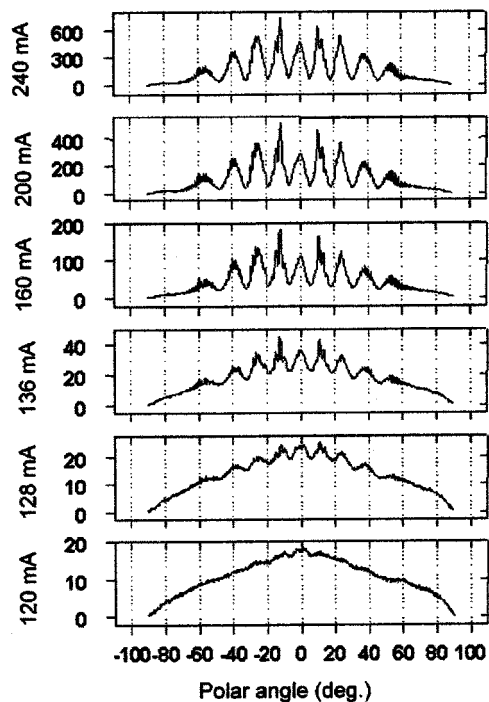


Fig. 6. The cross section of the emission patterns of typical 1-D modes in 2-D PC lasers as a function of the pumping power. The vertical axis titles indicate the driving current of the pumping LD which is proportional to the pumping power. The angular resolution of the measurements is 0.2° .

measurement. Below threshold, the interference fringes are buried in the total photoluminescence (PL). Above threshold, the interference fringes appear since the lasing mode dominates over other modes and the PL. In addition to the major fringes, a fine structure is resolved in the high-resolution angular scans. In fact, the fine structure appears as concentric rings whose spacing decreases as the polar angle increases in 2-D emission patterns. These concentric rings are reminiscent of Michelson interferometer rings which originate from the interference between the direct beam emitted upward and the secondary beam reflected at the interfaces below the laser structure. As a matter of fact, all far-field emission patterns contain such concentric rings whose spacing is different depending on the layered structure of the wafers.

4) *Polarization*: As described previously, the lasing modes in 2-D PC lasers are expected to be TE polarized. However, it should be noted that the far-field emission is not the lasing mode itself, but out-coupled radiation produced an interaction between the lasing mode and the 2-D PC. Therefore, simple polarization measurements of the integrated emission do not provide direct information on the polarization state of the lasing modes.

Fig. 7 shows polarization-resolved emission patterns of 1-D modes presented in Fig. 5. The experimental data displayed in the left columns indicate that both of the two transverse modes are linearly polarized along the fringes. In the simulation, TE-polarized coherent electric dipoles are placed at hole positions in the 2-D PC region [21]. Then, phase and intensity of the dipoles are optimized in the fitting process. As a result, we find that the wavevector of the lasing mode in the PC region is complex and the intensity decay length

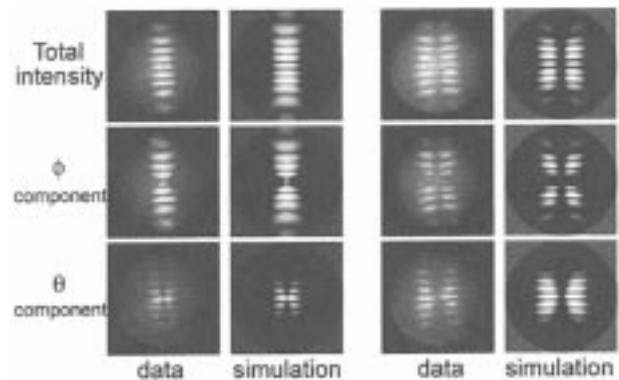


Fig. 7. The polarization-resolved emission patterns of the 2-D PC laser shown in Fig. 5. The simulation is based on the assumption that the lasing modes are transverse electric.

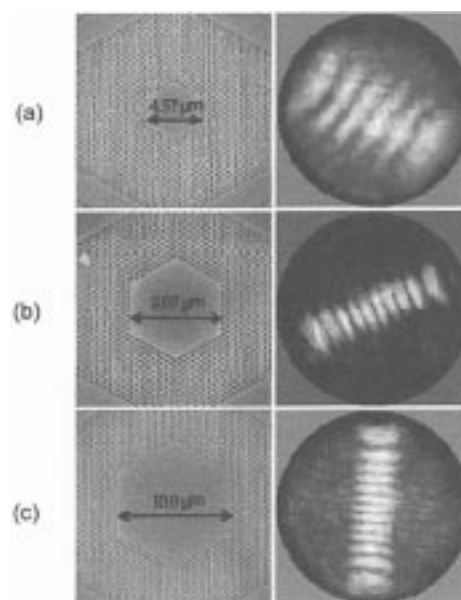


Fig. 8. The emission patterns of 1-D modes as a function of the cavity size. (a) A 13-defect cavity. (b) A 21-defect cavity. (c) A 29-defect cavity. The SEM images have the same magnification.

associated with its imaginary part is about the lattice constant. The simulation results with the best parameters are displayed in the right columns. Not only the intensity distributions, but also the two orthogonal polarization components, agree well with experimental data, so that the TE polarization of 1-D lasing modes is experimentally confirmed. Note that not magnetic dipoles but electric dipoles are used in the simulation. This is because the PC has a periodic modulation not in the magnetic permeability but in the electric permittivity.

5) *Cavity Sizes Versus Emission Patterns*: The emission patterns of various 1-D modes observed in: (a) 13-defect; (b) 21-defect; and (c) 29-defect cavities show different behaviors as shown in Fig. 8. The lattice constants are: (a) 370 nm; (b) 400 nm; and (c) 370 nm, respectively. The number of fringes increases as the cavity size increases, since the fringes are due to interference between two strong scattering regions formed at the cavity boundaries as described previously. Moreover, for a small cavity, the emission pattern becomes broader in the

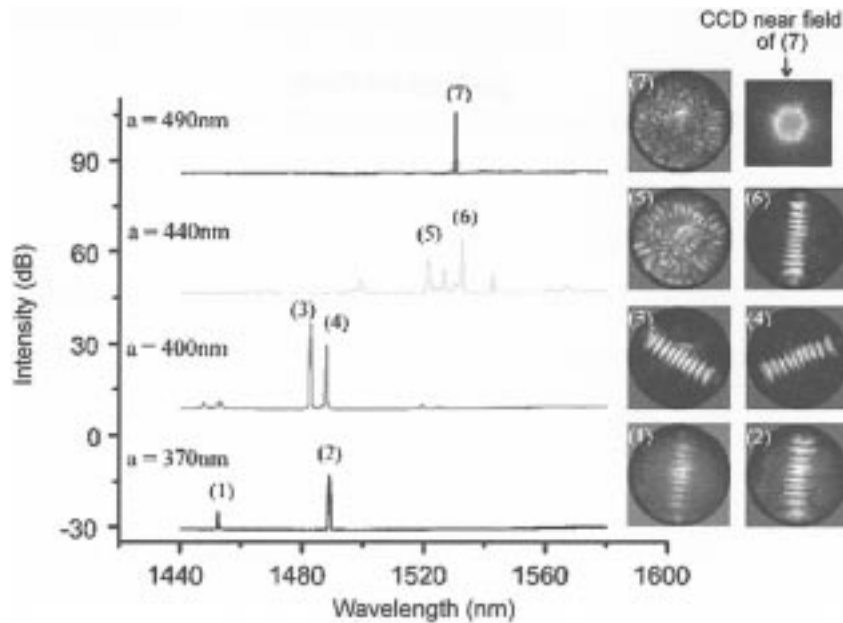


Fig. 9. The lasing modes observed in 21-defect cavities.

transverse direction because of the decrease of the mode size in that direction.

B. Two-Dimensional Modes

1) *Lattice Constants Versus Lasing Modes*: For 2-D PC cavities of larger lattice constants, we find that the lasers produce novel lasing modes which are genuinely 2-D. As the lattice constant increases, a certain transition from 1-D modes to 2-D modes is observed. The 21-defect cavities of different lattice constants are fabricated on one wafer and their lasing modes are observed. Lattice constants of the fabricated lasers are 370, 400, 440, and 490 nm and the hole radius is fixed to about $0.35 a$ in order to investigate the effect of periodicity only. The experimentally observed lasing modes are summarized in Fig. 9. In the 370-nm and the 400-nm cavities, only 1-D modes lase. The two modes in the 370-nm cavity are adjacent longitudinal modes, as previously described. In the 400-nm cavity, 1-D lasing modes in two directions are observed. Their longitudinal modes are also narrowly seen in the spectrum. In the 440-nm cavity, several modes are found to lase and two of them are measured. The 2-D lasing mode whose emission pattern is completely different from those of 1-D modes appears at a shorter wavelength as compared to the 1-D mode. In the 490-nm cavity, only the 2-D mode lases. The CCD near-field image is displayed in the right side.

The 2-D modes observed in the cavities of large lattice constants present complicated emission patterns including azimuthal fringes, implying circulation of field energy along the boundary. Likewise, the CCD near-field image shows that the whole boundary contributes to laser emission and bright spots are formed along the boundary. Numerical simulations show that the hexagonal cavity supports a whispering-gallery-like mode which has as many antinodes as holes along the cavity boundary. In the emission patterns, however, the number of azimuthal fringes is about 33, which corresponds to half the number of holes along the cavity boundary (66). Further studies

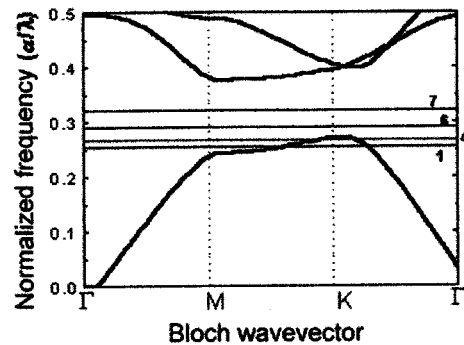


Fig. 10. The 2-D band structure corresponding to measured structures. An effective index of 2.8 is used in the plane-wave calculation. Normalized frequencies for the lasing modes (1), (4), (6), and (7) are represented as horizontal dotted lines.

on the out-coupling of lasing modes at their PC boundaries are necessary to explain this discrepancy.

In order to understand the observed results, the photonic band structure is investigated. The 2-D photonic band structure is calculated by using the plane-wave method with an effective refractive index of 2.8, shown in Fig. 10. The vertical axis of the band structure is a normalized frequency which means the ratio of the lattice constant to the free-space wavelength. Therefore, this value increases with the lattice constant for a fixed wavelength. The normalized frequencies for the lasing modes (1), (4), (6), and (7) are represented as horizontal lines in the band structure. It is interesting to note that the lasing wavelengths of (1) and (4) lie below the full in-plane bandgap. In this case, since these modes see the bandgap in the Γ -M direction, the modes show 1-D characteristics oscillating in the Γ -M direction. This interpretation agrees well with the observed results that the samples with a small lattice constant show only 1-D mode lasing actions. We do not observe 2-D lasing modes when the lattice constant is smaller than 400 nm. For modes (6) and (7), the lasing wavelength exists in the full bandgap region. In this case, both 1-D

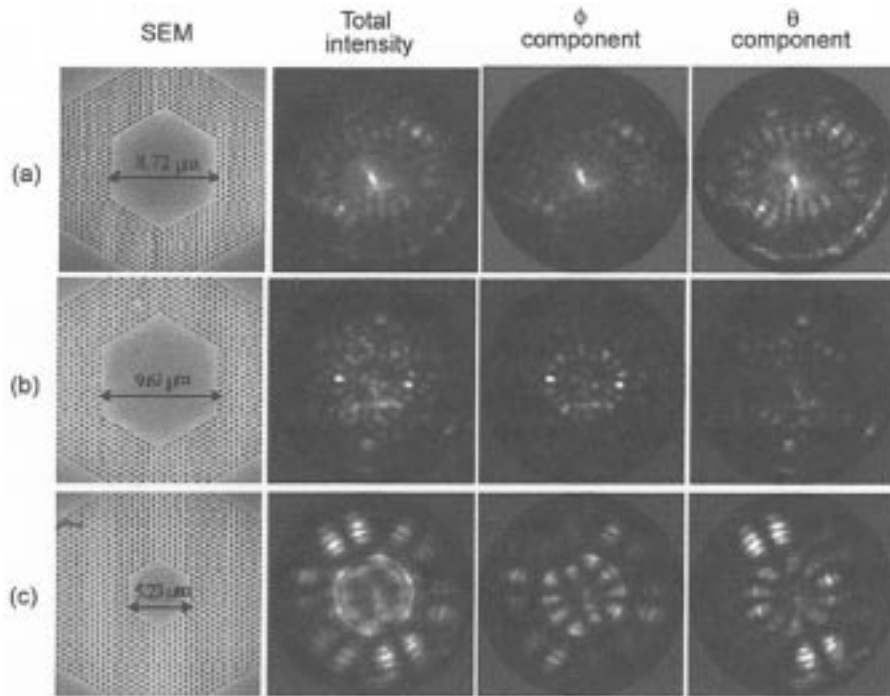


Fig. 11. Typical 2-D modes observed in 2-D PC lasers. (a) Lattice constant (a) = 460 nm, TM-like mode. (b) a = 500 nm, TE-like mode. (c) a = 500 nm, hybrid mode. The SEM images have the same magnification.

and 2-D modes can be observed. Modes (6) and (7) show 1-D and 2-D characteristics, respectively, as mentioned previously. Actually, for the samples with a large lattice constant, it is likely that the 2-D modes reach the lasing threshold more easily than the 1-D mode. This possibly implies that the 2-D modes have higher quality factors than does the 1-D mode.

2) *Polarization*: Polarization-resolved emission patterns are also investigated using various samples. The lattice constants and hole radii of the (a) 21-defect, (b) 21-defect, and (c) 11-defect cavities are 460 nm and $0.32a$, 500 nm and $0.29a$, and 500 nm and $0.31a$, respectively, in Fig. 11. The first mode (a) shows a circular emission pattern containing azimuthal fringes which are polarized along the θ direction. Therefore, this mode is TM-polarized even though the compressively strained quantum wells prefer TE polarization, as mentioned previously. The emission pattern of the second mode (b) is a combination of a ring which is polarized along the ϕ direction and a star which is polarized along the θ direction. The third mode (c) presents a sunflower-shaped emission pattern with 12 leaves. Eight leaves are polarized along the ϕ direction and four leaves are polarized along the θ direction. It should be emphasized that conventional polarization analyses obviously fail to reveal the polarization state of the 2-D modes. If the emission integrated by a lens is analyzed by a polarizer, the result should be an elliptical polarization dependent on the alignment of the lens.

IV. NEAR-FIELD RESULTS

A. One-Dimensional Modes

Fig. 12 presents near-field images of a 1-D lasing mode in a 31-defect cavity whose lattice constant and hole radius are 400 nm and $0.3a$, respectively. The 200×200 data points are

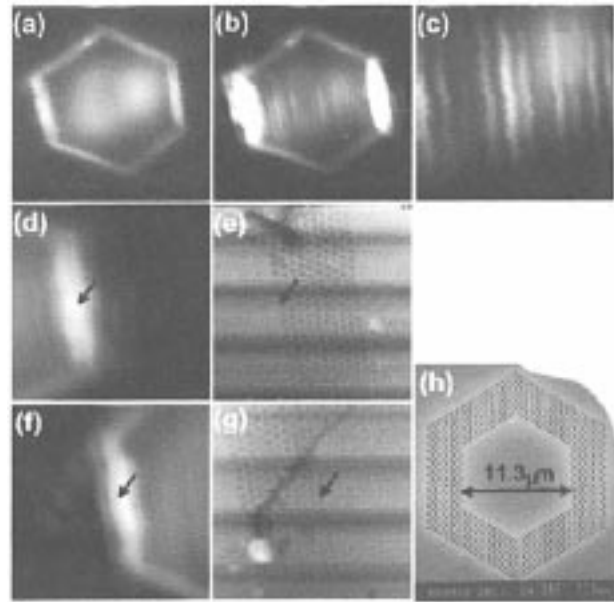


Fig. 12. NSOM images of 1-D lasing modes in a 2-D PC laser. (a) Below threshold. (b) Above threshold. (c) Fringes in the cavity region. (d) Zoom-in at the cavity boundary in the right side of (b). (e) Topography of (d). (f) Zoom-in at the cavity boundary in the left side of (b). (g) Topography of (f). (h) SEM image of the laser.

measured in the x and y directions. The SEM picture of the laser is shown in Fig. 12(h). In this measurement, the other end of a fiber probe is directly connected to a detector without the monochromator. The PL distribution below threshold is shown in Fig. 12(a). The bright region inside the cavity reflects the shape of the pumping spot which is optimized to achieve the lasing condition.

The near-field scan on the 1-D lasing mode above threshold is shown in Fig. 12(b). The two boundaries become dominantly strong and grating-like fringes parallel to the boundaries are observed inside the cavity. The 3-times magnified image of the fringe region is presented in Fig. 12(c). The fringe spacing is found to be ~ 770 nm which corresponds to $\lambda/2$. This means that the fringes are not evanescent tails of the lasing mode guided in the slab, but originated from the emission out-coupled to free space at the two boundaries. Therefore, the near-field fringes are artifacts, each of which directly corresponds to each of the far-field fringes discussed previously. This result implies that the uncoated probe is more sensitive to propagating fields than nonpropagating evanescent fields, presumably because the refractive index of the silica fiber probe ($n = 1.45$) is so low that optical tunneling from the high-index slab ($n = 3.4$) to the probe is relatively weak. Even though the near-field fringes are not real, they indicate that near-field probing by the uncoated silica fiber does not seriously perturb the lasing action of the PC laser.

Fig. 12(d)–(g) shows near-field images and their topographies simultaneously obtained near the right and left boundaries of Fig. 12(b), respectively. The arrows designate the same positions for comparison between the two images. The horizontal lines in the topographies are artifacts from the feedback electronics in the NSOM system. Fig. 12(d) and (f) shows that the near-field intensity decays within a few periods of the lattice in the PC region. As indicated by arrows, the bright region is mainly located inside the cavity in Fig. 12(d), while it is mainly located outside the cavity in Fig. 12(f), which reflects an asymmetry of the probe. Even though the drilled holes are well resolved in the topographies, the near-field images do not present a corresponding structure, especially along the boundaries. This implies that the propagating fields do not maintain the subwavelength structure even in the near-field regime. In order to reveal the subwavelength structure presumably associated with evanescent fields, it is necessary to use NSOM probes with metal cladding which blocks the coupling of propagating fields.

B. Two-Dimensional Modes

The near-field images shown in Fig. 13 are unambiguous demonstrations of the 2-D lasing mode (5). The lattice constant and the hole radius are 460 nm and $0.35a$, respectively. The 100×100 data points are measured in the x and y directions. In the total PL distribution of Fig. 13(a), the bright region inside the cavity reflects the shape of the pumping spot. The cavity boundary manifests itself as a continuous hexagon by scattering the light guided in the slab. It is interesting to see the resonant mode even below the threshold from spectrally resolved near-field measurements, as shown in Fig. 13(b). The hexagon is disconnected into segments corresponding to a few periods of the lattice along the boundary. Moreover, the bright pumping spot inside the cavity shown in Fig. 13(a) disappears in Fig. 13(b), suggesting that the resonant mode resides mainly along the boundary. Above threshold, the near-field distribution of the lasing mode is shown in Fig. 13(c). The segments become vivid and the contrast between bright and dark spots dramatically increases. The bright spots on the boundary seem to be the

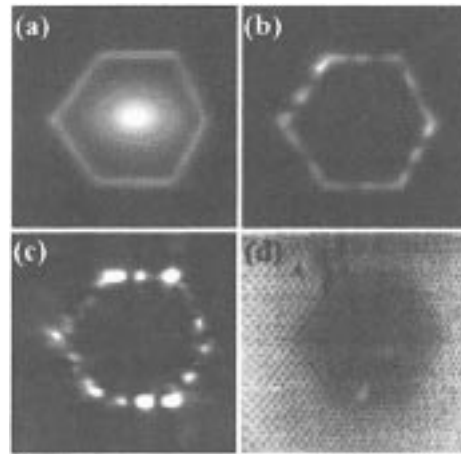


Fig. 13. NSOM images of the 2-D lasing mode (5) shown in Fig. 10. (a) Below threshold, total PL. (b) Below threshold, PL at 1520~1522 nm. (c) Above threshold, lasing at 1520~1522 nm. (d) Topography of (c).

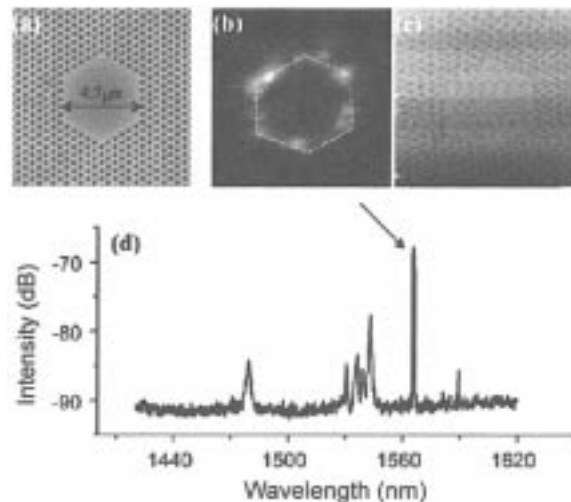


Fig. 14. (a) SEM images of the 2-D PC laser. (b) Near-field image of the 2-D lasing mode at 1566 nm. (c) Topography of (b). (d) Spectrum.

origin of azimuthal fringes observed in the far-field emission patterns.

In order to investigate the 2-D resonant modes more systematically, the variation of near-field distributions is traced over the whole spectral range of interest. Various lasers have been inspected in this way, and measurements from the 11-defect cavity shown in Fig. 14 are presented. This is the smallest laser in which a 2-D lasing mode is found. The lattice constant and the hole radius are 460 nm and $0.34 a$, respectively. This cavity has one 2-D lasing mode whose near-field image and lasing wavelength are shown in Fig. 14(b) and (d). It should be noted that the spectrum shown in Fig. 14(d) does not reveal all resonant modes, since the spectrum changes a lot as the pumping condition changes.

Spectrally resolved near-field images are tabulated in Fig. 15 every 7 nm with a 3-nm spectral window from 1402 to 1645 nm in wavelength. The 50×50 data points are measured in the x and y directions. The top-left image displays the total PL distribution, which is uniform overall in the cavity and along the boundary. Besides the lasing mode at 1566 nm, various resonant

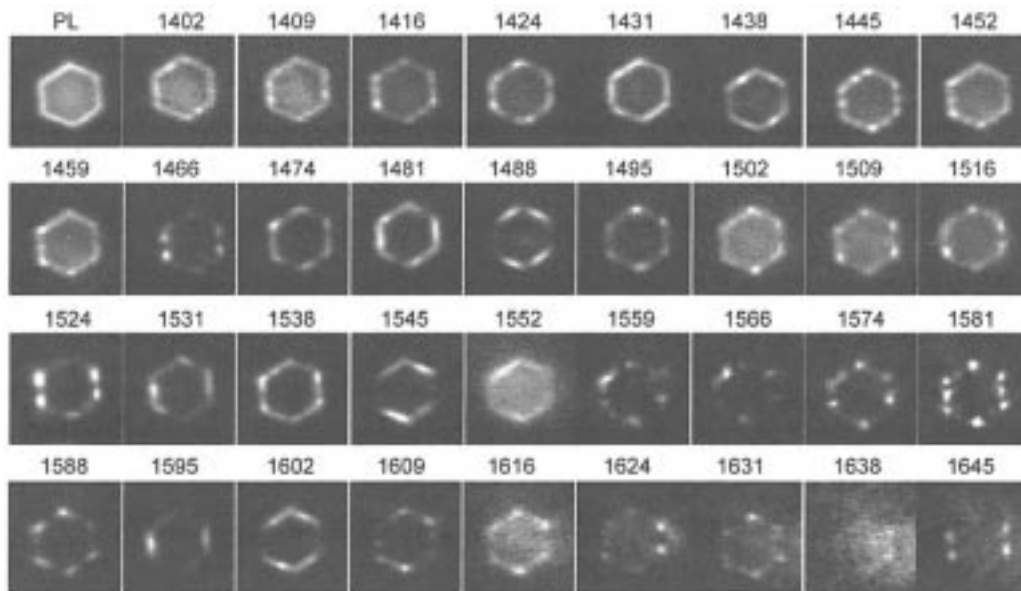


Fig. 15. Spectrally resolved near-field images of the 2-D PC laser shown in Fig. 15(a). The spectral resolution is 3 nm. The top-left image is the total PL distribution below threshold.

1-D and 2-D modes are discernible in the table. Although they cannot reach lasing threshold, 1-D resonant modes are observed at around 1431, 1488, 1545, and 1602 nm. They are separated by about 57 nm, which corresponds to the effective cavity length of $6.7 \mu\text{m}$ using a group refractive index of 3.0. This agrees well with the physical dimension of the cavity, taking into account the decay length of the lasing modes in the PC region. The modes at 1466, 1524, and 1645 nm can be also considered as transverse modes, since they have similar near-field distributions and they are separated by 57 or 114 nm. Some images show certain structures in poor contrast. This is presumably because nearly degenerate multiple modes are not spectrally resolved due to the large spectral window. The modes at 1424 nm and 1445 nm have circular field distributions which reminds one of the whispering gallery mode.

Since the 11-defect cavity consists of 91 defects, it supports hundreds of defect modes. This is confirmed by numerical calculations. It is interesting to know what kinds of modes are advantageous to lasing and how such modes can be classified. The current results provide basic insights into the various modes and can be fully understood on the basis of such theoretical analyses.

V. CONCLUSION

We have investigated the lasing modes in 2-D hexagonal cavities in the far- and near-field regimes and subsequently classified them into two categories, 1-D and 2-D modes, depending upon the nature of the lasing action. In the 1-D modes, the lasing occurs in between two parallel boundaries of the 2-D cavity. The degeneracy due to the 3-fold rotational symmetry is removed in actual cavities. The longitudinal and transverse modes are identified in the far-field emission patterns and their mirror symmetry is discussed. The polarization-resolved emission patterns and the simulation reveal that the 1-D modes are TE-polarized. The near-field images show that the lasing mode decays within a few periods in the PC region, and the propagating fields do

not maintain the subwavelength structure, once coupled to free space. The limitation of the uncoated fiber probe is also discussed. In the 2-D modes, the lasing oscillation occurs two-dimensionally so that the phenomena are rich compared to the 1-D modes. The far- and near-field images show that the 2-D modes have bright spots along the cavity boundary and they produce structures in the azimuthal direction in the emission patterns. The variety of the polarization states is illustrated by three special cases, the TM-like polarization, the TE-like polarization, and the hybrid state. In particular, spectrally resolved near-field images reveal that various 2-D resonant modes exist in the 2-D cavity and a few of them lase under certain conditions.

REFERENCES

- [1] J. D. Joannopoulos, P. R. Villeneuve, and S. Fan, "Photonic crystals: Putting a new twist on light," *Nature*, vol. 386, pp. 143–149, 1997.
- [2] E. Yablonovitch, "Inhibited spontaneous emission in solid-state physics and electronics," *Phys. Rev. Lett.*, vol. 58, pp. 2059–2062, 1987.
- [3] O. Painter, R. K. Lee, A. Scherer, A. Yariv, J. D. O'Brien, P. D. Dapkus, and I. Kim, "Two-dimensional photonic band-gap defect mode laser," *Science*, vol. 284, pp. 1819–1821, 1999.
- [4] O. J. Painter, A. Husain, A. Scherer, J. D. O'Brien, I. Kim, and P. D. Dapkus, "Room temperature photonic crystal defect lasers at near-infrared wavelengths in InGaAsP," *J. Lightwave Technol.*, vol. 17, pp. 2082–2088, 1999.
- [5] J. K. Hwang, H. Y. Ryu, D. S. Song, I. Y. Han, H. W. Song, H. K. Park, Y. H. Lee, and D. H. Jang, "Room-temperature triangular-lattice two-dimensional photonic band gap lasers operating at $1.54 \mu\text{m}$," *Appl. Phys. Lett.*, vol. 76, pp. 2982–2984, 2000.
- [6] J. K. Hwang, H. Y. Ryu, D. S. Song, I. Y. Han, H. K. Park, D. H. Jang, and Y. H. Lee, "Continuous room-temperature operation of optically pumped two-dimensional photonic crystal lasers at $1.6 \mu\text{m}$," *IEEE Photon. Technol. Lett.*, vol. 12, pp. 1295–1297, 2000.
- [7] M. Meier, A. Mekis, A. Dodabalapur, A. Timko, R. E. Slusher, J. D. Joannopoulos, and O. Nalamasu, "Laser action from two-dimensional distributed feedback in photonic crystals," *Appl. Phys. Lett.*, vol. 74, pp. 7–9, 1999.
- [8] S. Riechel, C. Kallinger, U. Lemmer, J. Feldmann, A. Gombert, V. Wittwer, and U. Scherf, "A nearly diffraction limited surface emitting conjugated polymer laser utilizing a two-dimensional photonic band structure," *Appl. Phys. Lett.*, vol. 77, pp. 2310–2312, 2000.

- [9] M. Notomi, H. Suzuki, and T. Tamamura, "Directional lasing oscillation of two-dimensional organic photonic crystal lasers at several photonic band gaps," *Appl. Phys. Lett.*, vol. 78, pp. 1325–1327, 2001.
- [10] M. Imada, S. Noda, A. Chutinan, T. Tokuda, M. Murara, and G. Sasaki, "Coherent two-dimensional lasing action in surface-emitting laser with triangular-lattice photonic crystal structure," *Appl. Phys. Lett.*, vol. 75, pp. 316–318, 1999.
- [11] P. R. Villeneuve, S. Fan, and J. D. Joannopoulos, "Microcavities in photonic crystals: Mode symmetry, tunability, and coupling efficiency," *Phys. Rev. B*, vol. 54, pp. 7837–7842, 1996.
- [12] S. G. Johnson, S. Fan, P. R. Villeneuve, and J. D. Joannopoulos, "Guided modes in photonic crystal slabs," *Phys. Rev. B*, vol. 60, pp. 5751–5758, 1999.
- [13] O. Painter, J. Vučković, and A. Scherer, "Defect modes of a two-dimensional photonic crystal in an optically thin dielectric slab," *J. Opt. Soc. Amer. B*, vol. 16, pp. 276–285, 1999.
- [14] A. M. Zheltikov, S. A. Magnitskii, and A. V. Tarasishin, "Two-dimensional photonic crystals with a lattice defect: Spectrum of defect modes, localization of light, and formation of evanescent waves," *J. Exp. Theoret. Phys.*, vol. 90, pp. 600–608, 2000.
- [15] H. Y. Ryu, J. K. Hwang, and Y. H. Lee, "Conditions of single guided mode in two-dimensional triangular photonic crystal slab waveguides," *J. Appl. Phys.*, vol. 88, pp. 4941–4946, 2000.
- [16] M. Meier, A. Dodabalapur, J. A. Rogers, R. E. Slusher, A. Mekis, A. Timko, C. A. Murray, R. Ruel, and O. Nalamasu, "Emission characteristics of two-dimensional organic photonic crystal lasers fabricated by replica molding," *J. Appl. Phys.*, vol. 86, pp. 3502–3507, 1999.
- [17] D. J. Shin, A. Chavez-Pirson, S. H. Kim, S. T. Jung, and Y. H. Lee, "Diffraction by a subwavelength-sized aperture in a metal plane," *J. Opt. Soc. Am. A*, vol. 18, pp. 1477–1486, 2001.
- [18] H. Y. Ryu, J. K. Hwang, D. S. Song, I. Y. Han, Y. H. Lee, and D. H. Jang, "Effect of nonradiative recombination on light emitting properties of two-dimensional photonic crystal slab structures," *Appl. Phys. Lett.*, vol. 78, pp. 1174–1176, 2001.
- [19] D. J. Shin, S. T. Jung, M. S. Lee, and Y. H. Lee, "New scheme for shear-force detection in NSOM based on a dual tuning fork system," in *Int. Conf. on Scanning Tunneling Microscopy*, Korea, 1999.
- [20] H. Y. Ryu, J. K. Hwang, and Y. H. Lee, "Effect of size nonuniformities on the band gap of two-dimensional photonic crystals," *Phys. Rev. B*, vol. 59, pp. 5463–5469, 1999.
- [21] C. J. M. Smith, T. F. Krauss, H. Benisty, M. Rattier, C. Weisbuch, U. Oesterle, and R. Houdré, "Directionally dependent confinement in photonic-crystal microcavities," *J. Opt. Soc. Amer. B*, vol. 17, pp. 2043–2051, 2000.

Dong-Jae Shin was born in An-dong City, Korea, in 1973. He received the B.S., M.S., and Ph.D. degrees from the Department of Physics, Korea Advanced Institute of Science and Technology (KAIST), Taejon, Korea, in 1995, 1997, 2001, respectively. During his Ph.D. work, his research focused on near-field optics, photonic crystal lasers, and microdisk lasers.

He is currently working on optical switching at Bell Laboratories, Lucent Technologies, Murray Hill, NJ, as a Post-Doctoral Member of Technical Staff. Dr. Shin is a member of the Optical Society of Korea (OSK).

Se-Heon Kim was born in Seoul City, Korea, in 1978. He received the B.S. degree from the Department of Physics, Korea Advanced Institute of Science and Technology (KAIST), Taejon, Korea, in 2000. He is currently working toward the M.S. degree at the same institution, studying resonant modes in photonic crystal ring-type cavities.

Jeong-Ki Hwang received the B.S., M.S., and Ph.D. degrees from the Department of Physics, Korea Advanced Institute of Science and Technology (KAIST), Taejon, Korea, in 1994, 1996, and 2000, respectively. During his Ph.D. work, he studied spontaneous and stimulated emission control in photonic bandgap cavities.

Han-Youl Ryu was born in Taegu City, Korea, on January 1, 1974. He received the B.S. and M.S. degrees from the Department of Physics, Korea Advanced Institute of Science and Technology (KAIST), Taejon, Korea, in 1996 and 1998, respectively. He is currently working toward the Ph.D. degree at the same institution.

His research interests include the design, fabrication, and characterization of photonic crystal light-emitting structures.

Hong-Gyu Park was born in Seoul City, Korea, in 1976. He received the B.S. and M.S. degrees from the Department of Physics, Korea Advanced Institute of Science and Technology (KAIST), Taejon, Korea, in 1998 and 2000, respectively. He is currently working toward the Ph.D. degree at the same institution, studying photonic crystal light-emitting structures.

Dae-Sung Song was born in Seosan City, Korea in 1972. He received the B.S. degree in 1996, from the Department of Physics, Korea University, Seoul, Korea, and the M.S. degree in 1998, from the Department of Physics, Korea Advanced Institute of Science and Technology (KAIST), Taejon, Korea, where he is currently working toward the Ph.D. degree and studying long-wavelength vertical-cavity surface-emitting lasers (VCSELs) and photonic crystal VCSELs.

Yong-Hee Lee received the M.S. degree in applied physics from the Korea Advanced Institute of Science and Technology (KAIST) and the Ph.D. degree in optical sciences from the University of Arizona, Tucson.

During his stay at AT&T Bell Laboratories, he demonstrated the first proton-implanted vertical-cavity surface-emitting lasers (VCSELs) in 1990 and holds the original patent on this industrial VCSEL. He has continued his research on VCSELs after he joined the Department of Physics of KAIST in 1991. Recently, his main interest lies in thresholdless photonic bandgap lasers and nanophotonic integrated optical circuits. He has co-authored more than 90 international journal papers and patents related to VCSELs and photonic bandgap structures.